Published in final edited form as:
Brain Res. 2009 January 9; 1247: 196–211. doi:10.1016/j.brainres.2008.10.015.

Tamoxifen mediated estrogen receptor activation protects against early impairment of hippocampal neuron excitability in an oxygen/glucose deprivation brain slice ischemia model

Huaqiu Zhang[1,3], **Minjie Xie**[1,4], **Gary P. Schools**[1], **Paul F. Feustel**[2], **Wei Wang**[4], **Ting Lei**[3], **Harold K. Kimelberg**[1], and **Min Zhou**[1,*]

1 *Neural and Vascular Biology, Ordway Research Institute, Center for Medical Science, 150 New Scotland Ave, Albany, NY 12208, USA*

2 *Center for Neuropharmacology and Neuroscience, Albany Medical College, Albany, NY 12208, USA*

3 *Department of Neurosurgery, Tongji Hospital, Tongji Medical College, Huazhong, University of Science and Technology, Wuhan, 430030, P.R. China*

4 *Department of Neurology, Tongji Hospital, Tongji Medical College, Huazhong, University of Science and Technology, Wuhan, 430030, P.R. China*

Abstract

Pretreatment of ovarectomized rats with estrogen shows long-term protection via activation of the estrogen receptor (ER). However, it remains unknown whether activation of the ER can provide protection against early neuronal damage when given acutely, we simulated ischemic conditions by applying oxygen and glucose deprived (OGD) solution to acute male rat hippocampal slices and examined the neuronal electrophysiological changes. Pyramidal neurons and interneurons showed a time-dependent membrane potential depolarization and reduction in evoked action potential frequency and amplitude over a 10 to 15 minute OGD exposure. These changes were largely suppressed by 10 μM TAM. The TAM effect was neuron-specific as the OGD induced astrocytic membrane potential depolarization was not altered. The TAM effect was mediated through ER activation because it could be simulated by 17β-estradiol and was completely inhibited by the ER inhibitor ICI 182, 780, and is therefore an example of TAM's selective estrogen receptor modulator (SERM) action. We further show that TAM effects on OGD- induced impairment of neuronal excitability was largely due to activation of neuroprotective BK channels, as the TAM effect was markedly attenuated by the BK channel inhibitor paxilline at10 μM. TAM also significantly reduced the frequency and amplitude of AMPA receptor mediated spontaneous excitatory postsynaptic currents (sEPSCs) in pyramidal neurons which is an early consequence of OGD. Altogether, this study demonstrates that both 17β-estradiol and TAM attenuate neuronal excitability impairment early on in simulated ischemia model via ER activation mediated potentiation of BK K^+ channels and reduction in enhanced neuronal AMPA/NMDA receptor-mediated excitotoxicity.

*Corresponding author: Min Zhou, Ph.D., Neural and Vascular Biology, Ordway Research Institute, 150 New Scotland Ave., Albany, NY 12208, Phone: (518) 641-6419; Fax: (518) 641-6304; E-mail: mzhou@ordwayresearch.org.

Keywords

tamoxifen; estrogen receptor; oxygen-glucose deprivation; neuronal excitability; acute hippocampus slice; neurons; astrocytes

1. INTRODUCTION

Brain ischemia or stroke is caused by partial or complete occlusion of cerebral blood flow to the brain. The loss of nutrients and oxygen initiates a devastating cascade starting from excessive excitatory amino acid release, followed by Ca^{2+}-overloading and breakdown of other transmembrane ion gradients, leading to early dysfunction of neuronal signaling and ultimately to brain dysfunction (Hansen, 1985; Rothman and Olney, 1986; Sweeney, 1995; Leis et al., 2005). Unfortunately, there are still no compounds approved for clinical use that could be beneficial to protecting neurons after ischemic stroke (Kozilo and Feng, 2006; Muir and Teal, 2005).

Tamoxifen (TAM) has been well-known as a selective estrogen receptor modulator (SERM) and its agonist or inhibitor actions on estrogen receptor (ER) vary among different tissues (Dhandapani and Brann, 2002). TAM has been identified as a potent neuroprotective compound *in vivo* and some of its likely mechanisms of action have been identified (Wakade et al., 2008; Zhang et al., 2005; Feustel et al., 2004; Osuka et al., 200; Kimelberg et al., 2000, 2003). However, whether and how the *in vivo* neuroprotection by TAM links to this important SERM action is not yet defined. Obviously, the mechanistic understanding on this issue will be helpful for further evaluation for clinical usefulness and design of more useful derivatives.

In the face of ischemic insults, voltage- and Ca^{2+} -activated K^+ channels (BK channels) are activated to reduce ischemic damage by maintaining neuronal membrane potential (Runden-Pran et al., 2002), and the activity of neuronal BK channels can be directly enhanced by 17β-estradiol (Nishimura et al., 2008). An event occurring very early in ischemia pathology and associating with neuronal membrane potential depolarization is the increase in spontaneous glutamate and GABA neurotransmitter release (Fleidervish et al., 2001) that lead to enhanced excitatory and inhibitory postsynaptic currents (EPSC and IPSC) (Allen and Attwell, 2004; Katchman and Hershkowitz, 1993). Such an enhanced activation of glutamate AMPA/NMDA receptors should lead to Na^+/Ca^{2+} overloading contributing to early neuronal damage. Based on these studies, we here ask whether a SERM action underlies the TAM neuroprotection that could start early in simulated ischemic conditions *in vitro* through potentiating BK channels and inhibiting excessively induced sEPSCs during ischemia.

The various *in vivo* ischemic models have clear advantages for determining neuroprotection through examining tissue damage and behavior changes in the intact animal. However, the questions of whether ER related neuroprotection action occurs early in ischemia and its underlying cellular mechanisms can be more precisely studied in the acute brain slice model, as we reported recently for resveratrol study (Zhang et al., 2008). Similarly, in this study OGD solution was applied to acute rat hippocampus slices to simulate ischemia *in vivo*, and whole-cell electrophysiological recording was performed to examine OGD-induced electrophysiology changes in hippocampal pyramidal neurons, interneurons and astrocytes from the *stratum radiatum*. We found that in the early OGD phase TAM like 17β-estradiol stimulates ER leading to retention of neuronal excitability via potentiation of BK channels and inhibition of ischemia-induced early increase in sEPSCs.

2. Results

2.1. Identification of pyramidal neurons, interneurons and astrocytes in acute hippocampal slices

Neurons and astrocytes in the hippocampal CA1 region can be morphologically distinguished when visualized via infrared differential interference contrast (IR-DIC) microscopy (Fig. 1A). Pyramidal neurons are located in the pyramidal layer with a characteristic soma shape and a long apical dendrite, extending from each soma and running into the *stratum radiatum* (*SR*). Interneurons in the *SR* have a large irregular soma and multiple dendrites. Astrocytes have smaller soma (≤10 μm diameter) with one or two primary processes visible in IR-DIC extending from the soma. In order to further determine the cell identities, we added 0.1% biocytin into the recording electrode solution for post-recording morphological study. For this purpose, the hippocampal slices were fixed in 4% formaldehyde immediately after whole cell recording and then subjected to immunohistochemistry. The resulting staining was viewed by laser scanning confocal microscopy (see Methods). The morphological characteristics of filled neurons and astrocytes were more clearly revealed by intracellular Cy2-streptavidin labeling of biocytin. The staining results from 6 biocytin filled pyramidal neurons, 5 interneurons and 5 astrocytes all confirmed that the initial cell type identification based on the differences in soma morphologies corresponded to the detailed morphological criteria for defining pyramidal neurons, interneurons and astrocytes revealed by the filled cells. Representative images for pyramidal neuron, interneuron and astrocyte and their corresponding electrophysiological recordings are shown in Fig. 1B–I.

As we recently reported that the identity of neurons and astrocytes was further supported by their distinctive electrophysiological characteristics. Both pyramidal neurons and interneurons were characterized by sequential activation of depolarization-induced large voltage-gated inward Na^+ and voltage-gated outward K^+ channel currents in voltage clamp recording. In addition, interneurons typically showed repetitive inward Na^+ currents during a 25 ms depolarization step (Fig. 1F) (Zhang et al., 2008). Astrocytes predominantly expressed linear I–V relationship K^+ currents and this has been used as a criterion for selection of astrocytes in this study and to exclude NG2 (+) cells (Zhou et al., 2006) (Fig. 1G). In current-clamp recording, a positive current pulse injection (100–300 pA/100 ms) induced a series of spikes in both pyramidal neurons and interneurons. Astrocytes showed no spikes in response to the same current injection (Fig. 1J).

2.2. Activation of estrogen receptors attenuates early OGD induced impairment of pyramidal and interneuron excitability

In the present study, we first assessed the acute OGD induced impairment of pyramidal neuron excitability. Since pyramidal neurons showed an average resting membrane potential (RMP) of −59.3±0.2 mV (n=27), and an average membrane resistance (R_M) of 198±24 MΩ(n=17), only the cells that required less than 100 pA/5 ms for single spike induction were used, as this was the current necessary to bring the membrane potential (Vm) from RMP, ~−60 mV, to the Na^+ channel threshold (−40 mV). The need for currents higher than this might indicate a deteriorated seal resistance during whole-cell formation (Zhang et al., 2008).

Changes in neuronal excitability were studied by monitoring evoked spikes every 20 s from stably recorded cells (Fig 2A). The amount of positive currents was then increased to evoke 3–4 spikes within a 100 ms. pulse duration, so that changes in neuronal excitability could be compared (Fig. 2Aa, 2B-a). The cell to cell variation for the required currents varied from 200 – 300 pA for an identical 100 ms pulse duration (n= 25). The same neuronal excitability test was used in our recent study (Zhang et al., 2008).

After control recording for at least 5 min. in normal aCSF continuously bubbled with 95% O_2/5% CO_2 (Fig. 2A), the perfusing fluid was switched to an OGD solution bubbled with 95% N_2/5% CO_2. To reliably determine protective effects, it was necessary to find a time window during which OGD-induced damage to pyramidal neuron excitability remained reversible. A preliminary study from 10 pyramidal neuron recordings with varied OGD exposure times resulted in a maximal time window of 15 min. OGD exposure for a reversible neuronal excitability change. To further confirm this critical time point, we extended OGD exposure time to 20 min. The neuronal excitability was barely recovered in only 8 out of 17 pyramidal neuron recordings (47%), and the remaining neurons showed no recovery. Also among the recovered pyramidal neurons, the Vm depolarization reached to −38.6±1.9 mV (n=8) that was far more depolarized than for a 15 min. OGD treatment (see below). Therefore, we used 15 min. as the standard OGD exposure in the following experiments, unless indicated otherwise.

OGD impairment of pyramidal neuron excitability was shown by 1) the time-dependent Vm depolarization that amounted to a 10 mV positive shift of the end of 15 min. OGD (Fig. 2C); 2) a marked decline in induced spike number at the end of OGD treatment as compared to the initial control level (Fig 2D); 3) a 20 mV decrease in the first spike amplitude over the course of OGD (Fig 2E). In addition, the spike number was transiently increased between 7 to 11 min. of OGD which paralleled the moderate initial Vm depolarization (from −54 mV to −52 mV) (Fig. 2A–B). We considered this spike increase was attributed to the OGD-induced Vm depolarization that shifted Vm closer to the threshold of neuronal Na^+ channels.

We first used TAM to determine if there was an acute protective effect of estrogen receptor activation as it is known both to be protective in animal models of cerebral ischemia (Kimelberg, 2005; Kimelberg et al., 2000), and it can act as both an inhibitor and agonist for estrogen receptors (Dhandapani and Brann, 2002). In the presence of 10 μM TAM, only a 4 mV Vm depolarization was produced in the end of 15 min. OGD (59 mV in control *vs*. 55 mV in OGD+TAM) (Fig. 2C). An average of 3 mV hyperpolarization was noticeable in the first 10 min. recovery period in normal aCSF that was followed by repolarization to pre-OGD levels. TAM also almost completely inhibited the suppression of spike number caused by OGD (Fig. 2D). Interestingly, a significant decrease in spike number was still observed during post-OGD Vm hyperpolarization (Fig 2B, C, D), indicating a direct impact of Vm on spike generation. In the presence of 10 μM TAM, the amplitude of the first spike decreased only from an average 94 mV to 86 mV (Fig. 2E), in contrast to an average drop of 20 mV seen in OGD alone (Fig. 2E). Since the decrease in action potential spike amplitude depended only on time and continued throughout the experiment in the TAM treatment group, this could be best explained as a time-dependent Na^+/K^+ channel run-down that commonly occurs in whole-cell recording, since most of our recordings lasted more than 50 min. after the establishment of whole-cell recording configuration.

To answer whether the TAM could retain neuronal excitability for longer than 15 min. in the OGD condition, we extended OGD exposure to 20 min. In the presence of 10 μM TAM, in 8 out of 10 recorded pyramidal neurons (80%) their excitability was recovered after a 20 min.OGD treatment (data not shown). The average Vm of those recovered recordings was −47.6±1.6 mV (n=8) which was much less depolarized as compared to those recordings with recovery after 20 min. OGD exposure without TAM (−38.6±1.9 mV, n=8, p <0.05). Also in the presence of TAM and OGD, the number of recordings that were able to recover from OGD insults also increased significantly (p <0. 05).

While TAM showed a strong effect in attenuating OGD induced pyramidal neuron excitability impairment, it would be interesting to know whether TAM would be able to retain neuronal excitability when OGD induced Vm depolarization has already been established. However, application of 10 μM TAM 15 min after OGD exposure failed to attenuate already impaired

neuronal excitability (n=3, data not shown). Therefore, this result indicates that TAM could only act on neurons that remained in their functionally reversible stages.

Since 0.1% DMSO was used as the vehicle for TAM, separate experiments with the same amounts of DMSO were tested (n=4). These showed a similar Vm depolarization and spike number decrease by the end of 15 min. as in OGD exposure without DMSO. Despite a slight Vm hyperpolarization (−3.8±1.1 mV, n=5) in the post-OGD recovery period as compared to OGD alone, the difference was not statistically significant. Therefore, DMSO was unlikely to contribute to the observed TAM action.

As noted above TAM is considered a selective estrogen receptor modulator (SERM) because it has both antagonist and agonist effects on estrogen receptors (ER), depending on the tissue (Dhandapani and Brann, 2002). To clarify whether acute TAM action described here is mediated through an ER agonist action, we used the high affinity, pure estrogen receptor inhibitor ICI 182, 780 (Wade et al., 1993). As the representative recording in Fig. 3A shows, the 10 μM TAM effect was completely inhibited by 1 μM ICI 182, 780 (n=6). To further confirm that TAM exerts an agonist action on ER, we added the pure estrogen receptor agonist 17β-estradial (1 μM) with OGD. 1 μM 17β-estradial produced a similar effect as 10 μM TAM (Fig. 6B). The mean effects of 1 μM 17β-estradial on several pyramidal neurons are summarized in Fig. 3C, D. The ER dependency of TAM action on neuronal excitability has been further confirmed by performing Tukey's HSD multiple comparison test and the further details are described in Fig. 3 and its legend.

We also sought to see whether TAM affords a similar action to OGD induced interneuron damage. Interneurons appeared more vulnerable to OGD insults, since a 15 min. OGD exposure resulted in irreversible damage to interneuron excitability (n=5, not shown). Therefore, for interneurons, we shortened the OGD exposure time to 10 min. The interneurons required less positive current (150±50 pA, n=12) to evoke 3–4 spikes, as compared to pyramidal neurons. Likely, this was due to a more depolarized RMP (−53±1.4 mV, n=12) and a relatively smaller interneuron cell size as indicated by the difference in membrane capacitance (Cm) between pyramidal neurons (83±18 pF, n=17) and interneurons (63±13.7 pF, n=8). Otherwise the experimental procedures were the same as for studying pyramidal neurons, as described above. As shown in Fig. 4 TAM produced a complete inhibition on the OGD induced interneuron Vm depolarization, spike number decrease and spike amplitude decline in interneurons.

Although interneurons appeared to be more sensitive to OGD insults and the TAM effect was more potent, we were also aware from our experiments and the literature that interneurons were morphologically and functionally very diverse in CA1 *stratum radiatum* (Somogyi and Klausberger, 2005). Thus, without adding additional interneuron subtype markers to discriminate subtypes, we cannot say whether the changes seen were specific to any interneuron subtype. Therefore, in the subsequent neuronal studies, we focused on CA1 pyramidal neurons as they are homogeneous in terms of their morphology and electrophysiology.

2.3. TAM showed no effect on OGD-induced astrocyte Vm depolarization

To see if TAM affects astrocyte responses to OGD, we examined OGD induced changes in astrocyte Vm during OGD in the presence and absence of TAM. The mature astrocytes were identified based on their expression of linear I–V relationship K^+ conductance (Zhou et al., 2006). The current clamp recording model was used to monitor astrocyte Vm changes during OGD exposure. It appeared that astrocytes are much more resistant to OGD as a 30 min. OGD induced Vm depolarization was always readily reversible (Fig. 5A, C). The astrocyte responses to OGD treatment and the underlying pathological mechanisms were addressed in detail in a separate report (Xie et al., 2008). In brief, astrocyte Vm showed a multiphasic depolarization that can be subdivided into at least two phases (Fig.5A). Upon OGD withdrawal, this

depolarized astrocyte Vm rapidly repolarized with a transient hyperpolarization evident in every recording (n=4). 10 μM TAM produced no significant effect on this characteristic astrocyte response to OGD (n=3) (Fig. 5B, C).

2.4. TAM suppresses the OGD induced increases in spontaneous EPSCs

An important part of TAM's effect on neuronal excitability seems to be through keeping the Vm close to control levels and it is well-known that Vm depolarization causing neuronal overexcitation is one of the major deleterious factors for acute hypoxia/ischemia damage (Rothman and Olney, 1986; Sweeney, 1995). Therefore, we next sought to determine whether TAM affects OGD-induced enhancement of spontaneous postsynaptic currents (sEPSCs) (Allen et al., 2004; Katchman and Hershkowitz., 1993). For sEPSC measurement, the Na^+ channels of the recorded cells were inhibited by adding QX-314 in the pipette solution. $GABA_A$ receptor-mediated inhibitory postsynaptic currents (IPSCs) were blocked by adding 25 μM bicuculline to the bath solution. When the pyramidal neurons were voltage-clamped close to their resting membrane potential (−60 mV), OGD induced a time-dependent downward shift in holding currents that was accompanied by an enhancement in the frequency and amplitudes of sEPSCs events (Fig. 6A). The representative segments from Fig. 6A at control, 10 min. and 15 min. of OGD are presented in expanded scale in Fig 6B. These sEPSCs are mostly mediated by AMPA-receptors at this holding potential (−60 mV) as these events were largely inhibited by the AMPA-R inhibitor NBQX (10 μM) (Fig. 6D, n=3). Since extracellular Mg^{2+} was present in the bath and the cells were clamped at −60 mV, an almost complete inhibition of sEPSCs by NBQX did not rule out the involvement of NMDA-R mediated sEPSCs that might be activated subsequent to AMPA-R activation in the absence of voltage clamping, as commonly occurs in excitatory synapses. In the presence of 10 μM TAM, these OGD induced sEPSCs changes were essentially completely inhibited (Fig. 6C). This TAM mediated inhibition of sEPSCs was compared with OGD alone by analyzing the cumulative fractions of sEPSCs amplitude and frequency with Synaptosoft software (Synaptosoft, Inc, GA, USA). As shown in Fig. 6E, TAM produced a significant left shift in the cumulative fraction curve of sEPSC events amplitude for the 15 min. OGD exposure. This indicated that the OGD-induced sEPSC amplitude was largely inhibited by TAM. The time-dependent inhibition of sEPSC frequency was also quantitatively compared between OGD alone and OGD plus TAM treatment groups and is shown in Fig 6F. In the presence of TAM, the OGD induced sEPSC frequency increase was considerably attenuated. Our results, therefore, not only confirmed previous findings that excessive sEPSCs can be induced by OGD, but also show that this can be almost completely inhibited by TAM.

2.5. TAM's action was partially mediated by potentiation of BK K^+ channels

BK channel activation plays a pivotal role in maintaining neuronal Vm in ischemia (Gong et al., 2000; Runden-Pran et al., 2002). Since the agonist action of TAM on ER leads to a sustained neuronal Vm in response to OGD (Fig. 3C), and ER activation can directly enhance BK channel activity (Nishimura et al., 2008), this promoted us to explore whether BK channel activation is a protective mechanism downstream of TAM-mediated ER activation.

Experimentally, the pyramidal neurons were voltage clamped at −60 mV during a 15 min OGD treatment. The black trace in Fig 7A shows the OGD-induced time-dependent downward shift in the holding currents, corresponding to neuronal Vm depolarization in current clamp recording. Of a total of 8 recorded neurons, the average holding current shift amounted to −82.9 ± 8.7 pA (n=8) after 15 min. of OGD. In the presence of 10 μM TAM (orange trace in Fig 8A), the OGD-induced inward current shift at the end of a 15 min. OGD exposure was inhibited by 72% with an average holding current shift of −23 ±5.7 pA (n=7). In the presence of the selective BK channel blocker, paxilline (Pax), at a saturating concentration of 10 μM (half maximal inhibition concentration ~10 nM, Gribkoff et al., 1996), TAM inhibition of the inward holding

current progression was reversed by 70% (green trace in Fig. 7B). We chose to use 10 μM Pax in our study as this was the concentration used in other brain slice studies where this concentration of Pax showed potent and specific inhibition of BK channels (Raffaelli et al., 2004;Benhassine and Berger, 2005). The average holding currents was −64.4±6.8 pA (n=8). 10 μM Pax alone did not produce inward current in recordings in normal aCSF solution (Fig. 7B, −9.7±5.9, n=4), consistent with the BK channel being inactive under physiological conditions (Gribkoff et al., 2001;Ghatta et al., 2006). This conclusion was further strengthened by applying 10 μM Pax with OGD, which gave the furthest inward shift in holding currents (inward current shift = −114.2±16.5, n=6, Fig. 8B), indicating that BK channels are only active under ischemic-type conditions. Further multiple comparisons for the results presented in Fig. 7B were performed using Tukey's HSD test; this allowed us to determine whether the differences amongst these groups were statistically significant (see Methods). Consistently, the differences between OGD/OGD+TAM, OGD+TAM/OGD+TAM+Pax and OGD+TAM/OGD+Pax groups were statistically significant (see legend in Fig. 7B).

TAM-induced inhibition of sEPSCs amplitude and frequency was only partially reversed by Pax (Fig 7C, D). Specifically, in the presence of Pax, TAM still significantly reduced the amplitude of sEPSCs (Fig. 7C), and the sEPSC frequency was also significantly reduced (Fig. 7D). By the end of 15 min. OGD, the sEPSC frequencies were 108.5 ± 8.8/min and 172.4 ± 6.4/min for TAM and TAM + Pax, representing a 57.3% (n=5) and 31.6% (n=6) of inhibition on OGD induced sEPSC events (253 ± 57/min, n= 5) at same time point, respectively.

2.6. OGD induced acute neuronal death was attenuated by TAM

To determine the extent to which OGD could cause neuronal death in the acutely prepared hippocampal slices and whether TAM treatment could prevent this neuronal death, we performed TO-PRO-3-I staining, as TO-PRO-3-I labels DNA in cells with compromised cell membranes (Van Hooijdonk et al., 1994) (see Methods). First, we found that 15 min. of OGD exposure did not produce a significant increase in TO-PRO-3-I staining as compared to the control (n=4). This is consistent with the preceding electrophysiological data that OGD-induced neuronal damage remained in a reversible phase. Exposure to OGD for 20 min., however, caused a marked 11.2±0.9 fold increase in TO-PRO-3-I staining density in the hippocampal CA1 pyramidal neurons layer as compared to control slices treated with aCSF for 20 min. (Fig. 8A). In the presence of 10 μM TAM in OGD solution, the difference was reduced to 6.4±0.4 fold as compared to OGD control group (Fig. 8B). Quantification of TO-PRO-3-I staining from 20 min OGD treatment in the presence and absence of TAM are shown in Fig. 8C. Although OGD also caused a noticeable TO-PRO-3-I staining in *stratum radiatum*, we found that we were unable to correlate these staining signals to interneurons and astrocytes specifically, so that we focused on the pyramidal neurons as this allowed us to assess OGD caused neuronal damage and TAM effects unambiguously.

3. Discussion

By showing that activation of ER by either TAM or 17β estradiol can exert an early inhibition of the OGD-induced impairment of neuronal excitability in hippocampal slices, our results demonstrate that part of the early TAM neuroprotection is offered by the SERM-type agonist action of TAM via ER. The ER activation is followed by potentiation of BK K^+ channels and inhibition of neuronal sEPSCs early in the ischemia.

3.1. OGD induced impairment of hippocampal neuronal excitability

It has been shown that OGD induces a two phase neuronal Vm depolarization in acute brain slices. The initial small reversible Vm depolarization (10–15 mV) lasts for 2–5 min. and is followed by a second large irreversible Vm depolarization (25–30 mV), termed anoxic

depolarization (AD) (Müller and Somjen, 2000; Hansen, 1985; Allen et al., 2005). We therefore studied the protective effects within the first reversible period. We also chose to use room temperature as the reversible neuronal depolarization phase is extended under these conditions (Morikawa et al., 1992; Taylor and Weber, 1993). According to the report by Onitsuka et al (1998) the reversible neuronal Vm depolarization phase can last for 14.4 min at 27 °C, which is consistent with our observation that the 15 min. OGD induced electrophysiological changes in hippocampal pyramidal neurons were readily reversible. This time window is consistent with our cell viability test, where the TO-PRO-3-I staining in pyramidal neuron was only markedly enhanced in 20 min OGD treatment group and not the 15 min. group. This time window is also consistent with the availability of stored energy in the slice that could last for ~ 11 min under OGD conditions (Xie et al., 2008). This allowed us to reliably examine any early effects of TAM on OGD-induced changes in neuronal excitability.

3.3. Estrogen receptor activation is responsible for the early protective effect on neuronal excitability

Part of TAM's protective action has been considered as a potent nonsteroid selective estrogen receptor modulator (SERM) that protects neurons via an agonist action on brain estrogen receptors, especially with pretreatment with TAM (Dhandapani and Brann, 2002). The present study clearly shows that early acute TAM action in retaining neuronal excitability was fully dependent on estrogen receptors, since β-estradiol produced the same TAM-like effect and TAM's effect was completely inhibited by the high affinity estrogen receptor inhibitor, ICI182, 780 (Fig, 3). The immediate TAM effect in attenuating impaired neuronal excitability strongly suggests a nongenomic action of TAM as genomic TAM effects require at least 24 hours to manifest themselves (Dhandapani and Brann, 2002; Dick et al., 2002). It would be of interest to determine in the future the specific nongenomic signaling pathways, such as MAPK and PI3-K (Kuroki et al., 2001), that might be involved in early TAM actions on neuronal excitability, and whether the α or β forms of the estrogen receptor are involved since both are expressed in the brain (Dhandapani and Brann, 2002). Technically, this would require a perforated patch recording mode for overcoming the pipette solution dialysis of the recorded neurons that interfere with these cytoplasmic signals, a limitation inherent in conventional open access whole-cell recording.

3.3. TAM attenuates OGD induced early neuronal membrane potential depolarization

Membrane potential depolarization has been considered as important index of the neuronal excitability depression occurring during ischemia, characterized by a sudden decrease in membrane potential, or an increase in inward holding currents when measured in the voltage clamp model (Raley-Susman et al., 2001; Allen et al., 2005). Ischemia-induced breakdown of transmembrane ion gradients, increase in neurotransmitter release and opening of hemichannels have all been suggested to account for this sudden Vm depolarization (Hansen 1985; Rossi et al., 2000; Thompson et al., 2006). In the present study, we have shown that ER activation can substantially sustain neuronal Vm during the early 10–15 min. of ischemia. Importantly, we show that the ER activation potentiates BK K^+ channels that attenuate OGD induced neuronal Vm depolarization. However, the BK channel inhibitor Pax blocked only about 70% of TAM produced neuronal Vm protection (Fig 7B), suggesting additional TAM actions should also be involved; these could include inhibition of excitatory amino acid release and antioxidative effects that have all been observed in the *in vivo* ischemia studies (Kimelberg et al, 2000, 2003; Osuka et al, 2001; Feustel, et al, 2004). Since TAM has been shown to directly activate BK channels in smooth muscle (Dick et al, 2002), additional issue that needs to be taken into account is to what extent TAM induced BK channel potentiation is mediated through estrogen receptor or by a direct effect on BK channels. In addition, since estrogen can directly modulate BK channels via ER activation, the signaling transduction pathway that mediates this fast ion channel activity change needs to be determined in future studies.

3.4. TAM inhibits spontaneous excitatory postsynaptic currents

The increase in spontaneous EPSCs (sEPSCs) in the OGD brain slice model has been reported to be due to excessive release of glutamate which acts on postsynaptic AMPA/NMDA receptors (Quintana et al., 2006; Katchman and Hershkowitz, 1994). The over-activation of postsynaptic AMPA/NMDA receptors also leads to neurotoxicity, and therefore the increase in sEPSCs has been considered as a marker of the earliest damage to neuronal function. In this study we showed that this OGD-induced excessive increase in sEPSCs was almost completely inhibited by TAM (Figs. 6, 7). By eliminating EPSCs TAM should be able to attenuate the neuronal excitotoxicity. Since the AMPA receptor channel pores in rat hippocampal pyramidal neurons consist of Ca^{2+} impermeable GluR1/GluR2 or GluR2/GluR3 tetramers (Plant et al., 2006), the fact that OGD induced sEPSC events were almost completely inhibited by the AMPA receptor inhibitor NBQX when the cells were clamped at − 60 mV (Fig. 7D), suggests that TAM mostly inhibited Na^+ influx into the patched pyramidal neurons through their AMPA receptors. However, it is conceivable that, in ischemia, the neuronal membrane potential would depolarize to a level sufficient enough to expel Mg^{2+} from NMDA channel pores resulting in additional Ca^{2+} influx through NMDA receptors.

3.5. Lack of effect of TAM on astrocyte membrane potential

We observed no TAM effect on astrocyte Vm depolarization due to OGD (Fig. 5), showing that the early TAM effects in the slice model are specific to neurons. The selective TAM action on neurons is unlikely caused by lack of estrogen receptor expression by astrocytes, since expression of equal amount of estrogen receptors by hippocampal astrocytes and neurons has been reported in a detailed EM study (Milner et al, 2005). Since astrocyte Vm depolarization in OGD mostly reflects increase in extracellular $[K^+]$, due to failure in Na^+-K^+ ATPase in both neurons and astrocytes (Xie et al., 2008), this finding also implies that TAM does not affect ischemia-induced increases in extracellular K^+. Apparently this is controversial if TAM inhibits OGD induced neuronal firing and the resulted excessive K^+ release, one would anticipate a decreased responses of astrocytic Vm depolarization. However, TAM mediated inhibition of neuronal firing is mediated by potentiation of BK, a well-known “emergency brake” mechanism that leads to enhanced K^+ efflux. This would well explain why the extracellular $[K^+]$ was essentially unchanged in astrocytic Vm measurement.

3.6. TAM action unlikely mediated by inhibiting of volume-regulated anion channels

TAM has been shown to be a potent inhibitor of volume-regulated anion channels (VRACs) in many cell types, including primary cultured astrocytes (Abdullave et al., 2006), but pyramidal cell VRACs in brain slices are insensitive to TAM (Inoue and Okada, 2007). It is still technically difficult to study astrocytic VRAC currents because of a lacking of specific inhibitors for the large two-pore domain K^+ channel mediated K^+ conductance expressed by astrocytes in brain slices (Zhou et al., 2006). However, if TAM inhibited the OGD-induced astrocytic VRAC currents in our study, one would anticipate seeing at least a partially decreased astrocyte Vm depolarization, as the result of TAM inhibition of Cl^- efflux through astrocytic VRACs (the equilibrium potential for Cl^- E_{Cl}= 0 mV). However, TAM showed no effect on OGD induced depolarization of astrocyte Vm, thus, the likelihood of a TAM action on neuronal and astrocytic VRACs that in turn mediates the acute TAM effect on neuronal excitability is low.

In conclusion, our results indicate that a SERM-type agonist action of TAM appear to be an early protective mechanisms exhibited by this highly protective compound to the animal stroke models. Mechanistically, potentiation of BK channels and inhibition of sEPSCs are downstream events following the TAM SERM action of activating ERs.

4. Experimental procedures

4.1. Hippocampal slice preparation

Acute hippocampal slices were prepared from 3–4 weeks old male Sprague-Dawley rats in accordance with a protocol approved by the Wadsworth Center, New York State Department of Health Institutional Animal Care and Use Committee. Animals were anesthetized with isoflurane before decapitation, and their brains were removed from the skull and placed in an ice-cold, oxygenated (5% CO_2-95%O_2, pH = 7.35) slice preparation solution containing (in mM) 26 $NaHCO_3$, 1.25 NaH_2PO_4, 2.5 KCl, 10 $MgCl_2$, 10 glucose, 0.5 $CaCl_2$, and 240 sucrose. Final osmolarity was 350 ± 2 mOsm. Coronal slices of 300 μm thickness were cut with a Vibratome 1500 (Ted Pella Inc., Redding, CA, USA) and transferred to a nylon-basket slice holder in artificial cerebral spinal fluid (aCSF) (20–22°C) containing (in mM) 125 NaCl, 25 $NaHCO_3$, 10 glucose, 3.5 KCl, 1.25 NaH_2PO_4, 2.0 $CaCl_2$, and 1.0 $MgCl_2$ (osmolarity, 295 ± 5 mOsm). The slices were allowed to recover in aCSF with continuous oxygenation for at least 60 min before recording.

4.2. Oxygen–glucose deprivation (OGD) procedure

Oxygen-glucose deprivation was achieved by substituting sucrose for D-glucose in aCSF and bubbling with 95% N_2 and 5% CO_2 for at least 30 min to deplete O_2 content and maintain pH values within 7.3–7.4. Bubbling was continued during the exposure of the slice to OGD solution in the recording chamber. In estradiol or TAM treatment groups, the chemicals were included in the OGD solution and applied to the slices at the beginning of each OGD treatment. The same OGD procedure has been used in our recent studies (Xie et al., 2008; Zhang et al., 2008).

4.3. Electrophysiology

For *in situ* recording, individual hippocampal slices were gently transferred into a recording chamber that was constantly perfused with oxygenated aCSF (2.5 ml/min). Whole-cell membrane currents in voltage clamp mode and potential in current clamp mode were amplified using a MultiClamp 700A amplifier, and the analog signals were sampled by a Digidata 1322A interface. The data acquisition was controlled by pCLAMP 9.0 software (Axon Instruments, Union City, CA) installed on a Dell personal computer. Low resistance patch pipettes were fabricated from borosilicate capillaries (OD: 1.5 mm; Warner Instrument Corporation, Hamden, CT) using a Flaming/Brown Micropipette Puller (Model P-87, Sutter Instrument Co., Novato, CA). When filled with K-gluconate-based electrode solution (see below), the electrode resistance was 3–5 MΩ. For all recordings, the initial seal resistance had to be greater than 3 GΩ for us to proceed to whole-cell recordings by rupturing the membrane with negative pressure pulses. Membrane potentials were read in the "*I*= 0" mode when recording was performed in voltage clamp mode, or continuously monitored in current clamp mode without current delivery. Membrane capacitance (*C*m) and electrode access resistances (*R*a) were measured using the "membrane test" protocol built into the pCLAMP 9.0. Only those recordings where the *R*a was below 15 MΩ and varied less than ±10% throughout the experiment were included in the final data analyses. Patch pipettes were filled with a solution containing (mM) 3 KCl, 137 K-gluconate, 0.5 $CaCl_2$, 1 $MgCl_2$, 5 EGTA, 10 HEPES, 3 Mg-ATP and 0.3 Na-GTP (pH was adjusted to 7.25–7.27 at 20°C with KOH, 280 ± 5 mOsm). All the experiments were conducted at room temperature (22–24°C).

4.4. Morphological studies

In some whole-cell recordings, biocytin (0.1%) was added into electrode solution to show the full morphology of pyramidal neurons, interneurons and astrocytes by post recording confocal microscopy. The hippocampal slices containing the biocytin-filled cells were then fixed right

after electrophysiological recording for 45 to 60 min in phosphate-buffered 4% formaldehyde, pH 7.4. After washing with phosphate buffered saline (PBS), the slices were permeabilized with 1.0% Triton X-100 in PBS (1 hr). In order to visualize the biocytin-filled cells the slices were treated with 1:1200 Cy2-streptavidin in PBS for 4 hours, followed by washing in PBS. Slices were viewed with a Zeiss LSM510 META confocal microscope with 10X/0.3n.a., 25X/0.8n.a., and 63X/1.4n.a. objectives. The recorded cell was initially found using a 50W mercury arc lamp with a 10X objective and a filter set for Cy2. The intensity of the Cy2 signal and the location of the mark made by the recording electrode were used to identify the recorded cell. In the laser scanning mode the Cy2 was excited and its emission was acquired. A differential interference contrast (DIC) image of each z plane was also acquired. Two dimensional projections of the image stacks were made using the LSM510 program.

4.5. TO-PRO-3 iodide staining and quantification of neuronal viability

The cell viability of acute hippocampal slices were determined by TO-PRO-3 iodide staining (TO-PRO-3-I) (Zhang et al., 2008). The level of TO-PRO-3-I incorporation into cellular DNA is indicative of significant membrane injury and has been widely used to distinguish dead cells from live cells (Van Hooijdonk et al., 1994). The acute hippocampal slices were prepared from P21 male rate according to the same procedure as for electrophysiological recording (n=3). In each preparation, 6–8 hippocampal slices obtained were first allowed to recover in aCSF for one hour and were then randomly divided into control (in normal aCSF), OGD and OGD +10 μM TAM groups. The slices were then placed into Petri dishes for 15 or 20 min. under the 1:2000 dilution of TO-PRO-3-I (Molecular Probes, Eugene, OR) from 1 mM stock solution. The slices were incubated at room temperature for 20 min. The TO-PRO-3-I staining in slices was then inspected with a Carl Zeiss LSM510 META confocal microscope using the 630 nm line of the HeNe laser. Emission was filtered through a long pass 650 nm filter. Image stacks were acquired from the slice surface to a depth of 30 μm, with the same acquisition settings used for all conditions. For data quantification, TO-PRO-3-I fluorescence above the background in the CA1 pyramidal layer was determined using the “density slice” option of National Institutes of the Health Image J program (Rasband 1997). In each experiment where the slices were obtained from the same preparation, the TO-PRO-3-I fluorescence densities from the control slices were defined as 100%, and TO-PRO-3-I fluorescence densities from the OGD and OGD+TAM were normalized to the control densities to calculate the percentage changes, as shown in Fig. 8.

4.6. Solutions and reagents

Tamoxifen-citrate, tamoxifen base, ICI-182780 and 17β-estradial were purchased from Sigma (St. Louis, MO, USA). NBQX, QX-314, bicuculline and paxilline were purchased from Tocris Bioscience (Ellisville, Missouri, USA). For preparation of stock solutions, NBQX, bicuculline and QX-314 were dissolved in water and the others were dissolved in DMSO and stored in a −20 °C freezer prior to use. These stock solutions were diluted to the final experimental concentration just before each experiment.

4.7. Data analysis

Data are presented as means ± SEM. Student’s *t*-test was performed to assess the statistical significance of the difference before and after treatment in the same experimental group. One-way ANOVA test was performed to determine the statistical significance of the differences between 2 experimental groups. Differences were considered significant at $p < 0.05$. Tukey’s HSD test was used for multiple comparisons with significance accepted at $p<0.05$ level using Statistica software (StatSoft, Inc, Tulsa, OK, USA).

The frequency and the cumulative fraction of the amplitudes of the spontaneous excitatory postsynaptic currents (sEPSCs) were analyzed using the Synaptosoft software (Synaptosoft, Inc, GA, USA).

Acknowledgements

This work was partially supported by National Institutes of Health Grants R01-NS35205 (to H.K.K), National Science Foundation grant ISO-0641828 (to M.Z). We thank Z-H Zhao for technical assistance, and Drs. I. Abdullayev and AA Mongin for helpful discussions.

References

1. Abdullaev IF, Rudkouskaya A, Schools GP, Kimelberg HK, Mongin AA. Pharmacological comparison of swelling-activated excitatory amino acid release and Cl-currents in cultured rat astrocytes. J Physiol 2006;572:677–89. [PubMed: 16527858]
2. Allen NJ, Attwell D. The effect of simulated ischaemia on spontaneous GABA release in area CA1 of the juvenile rat hippocampus. J Physiol 2004;561:485–98. [PubMed: 15459240]
3. Allen NJ, Karadottir R, Attwell D. A preferential role for glycolysis in preventing the anoxic sepolarization of rat hippocampal area CA1 pyramidal cells. J Neurosci 2005;25:848–859. [PubMed: 15673665]
4. Benhassine N, Berger T. Homogenous distribution of large-conductance calcium-dependent potassium channels on soma and apical dendrite of rat neocortical layer 5 pyramidal neurons. Eur J Neurosci 2005;21:914–26. [PubMed: 15787698]
5. Dhandapani KM, Brann DW. Protective effects of estrogen and selective estrogen receptor modulators in the brain. Biol Reprod 2002;67:1379–85. [PubMed: 12390866]
6. Dick GM, Hunter AC, Sanders KN. Ethylbromide tamoxifen, a membrane-impermeant antiestrogen, activates smooth muscle calcium-activated large-conductance potassium channels from the extracellular side. Mol Pharmacol 2002;61:1105–13. [PubMed: 11961128]
7. Feustel PJ, Jin Y, Kimelberg HK. Volume-regulated anion channels are the predominant contributors to release of excitatory amino acids in the ischemic cortical penumbra. Stroke 2004;35:1164–8. [PubMed: 15017010]
8. Fleiervish IA, Gebhardt C, Heinemann U. Enhance spontaneous transmitter release is the earliest consequence of neocortical hypoxia that can explain the disruption of normal circuit function. J Neurosci 2001;21:46000–8.
9. Ghatta S, Nimmagadda D, Xu X, O'Rourke ST. Large-conductance, calcium-activated potassium channels: structural and functional implications. Pharmacol Ther 2006;110:103–16. [PubMed: 16356551]
10. Gong L, Gao TM, Li X. Enhancement in activities of large conductance calcium-activated potassium channels in CA1 pyramidal neurons of rat hippocampus after transient forebrain ischemia. Brain Res 2000;24:147–54. [PubMed: 11082496]
11. Gribkoff VK, Lum-Ragan JT, Boissard CG, Post-Munson DJ, Meanwell NA, Starrett JE Jr, Kozlowski ES, Romine JL, Trojnacki JT, Mckay MC, Zhong J, Dworetzky SI. Effects of channel modulators on cloned large-conductance calcium-activated potassium channels. Mol Pharmacol 1996;50:206–17. [PubMed: 8700114]
12. Gribkoff VK, Starrett JE Jr, Dworetzky SI, Hewawasam P, Boissard CG, Cook DA, Frantz SW, Heman K, Hibbard JR, Huston K, Johnson G, Krishnan BS, Kinney GG, Lombardo LA, Meanwell NA, Molinoff PB, Myers RA, Moon SL, Ortiz A, Pajor L, Pieschl RL, Post-Munson DJ, Signor LJ, Srinivas N, Taber MT, Thalody G, Trojnacki JT, Wiener H, Yeleswaram K, Yeola SW. Targeting acute ischemic stroke with a calcium-sensitive opener of maxi-K potassium channels. Nat Med 2001;7:71–477.
13. Gu N, Vervaeke K, Storm JF. BK potassium channels facilitate high-frequency firing and cause early spike frequency adaptation in rat CA1 hippocampal pyramidal cells. J Physiol 2007;580:859–82. [PubMed: 17303637]
14. Hansen AJ. Effect of anoxia on ion distribution in the brain. Physiol Rev 1985;65:101–148. [PubMed: 3880896]

15. Inoue H, Okada Y. Roles of volume-sensitive chloride channel in excitotoxic neuronal injury. J Neurosci 2007;27:1445–55. [PubMed: 17287519]

16. Katchman AN, Hershkowitz N. Early anoxia-induced vesicular glutamate release results from mobilization of calcium from intracellular stores. J Neurophysiol 1993;70:1–7. [PubMed: 8103087]

17. Katchman AN, Hershkowitz N. Arachidonic acid participates in the anoxia-induced increase in mEPSC frequency in CA1 neurons of the rat hippocampus. Neurosci Lett 1994;28:217–20. [PubMed: 8028779]

18. Kimelberg HK. Astrocytic swelling in cerebral ischemia as a possible cause of injury and target for therapy. Glia 2005;50:389–397. [PubMed: 15846797]

19. Kimelberg HK, Feustel PJ, Jin Y. Acute treatment with tamoxifen reduces ischemic damage following middle cerebral artery occlusion. Neuroreport 2000;11:2675–2679. [PubMed: 10976942]

20. Kimelberg HK, Jin Y, Charniga C. Neuroprotective activity of tamoxifen in permanent focal ischemia. J Neurosurg 2003;99:138–142. [PubMed: 12854756]

21. Koziol JA, Feng AC. On the analysis and interpretation of outcome measures in stroke clinical trials: lessons from the SAINT I study of NXY-059 for acute ischemic stroke. Stroke 2006;37:2644–7. [PubMed: 16946150]

22. Kuroki Y, Fukushima K, Kanda Y, Mizuno K, Watanabe Y. Neuroprotection by estrogen via extracellular signal-regulated kinase against quinolinic acid-induced cell death in the rat hippocampus. Eur J Neurosci 2001;13:472–6. [PubMed: 11168553]

23. Leis JA, Bekar LK, Walz W. Potassium homeostasis in the ischemic brain. Glia 2005;50:407–16. [PubMed: 15846795]review

24. Milner TA, Ayoola K, Drake CT, Herrick SP, Tabori NE, McEwen BS, Warrier S, Alves SE. Ultrastructural localization of estrogen receptor beta immunoreactivity in the rat hippocampal formation. J Com Neurol 2005;491:81–95.

25. Morikawa E, Ginsberg MD, Dietrich WD, Duncan RC, Kraydieh S, Globus MY, Busto R. The significance of brain temperature in focal cerebral ischemia: histopathological consequences of middle cerebral artery occlusion in the rat. J Cereb Blood Flow Metab 1992;12:380–9. [PubMed: 1569134]

26. Muir KW, Teal PA. Why have neuroprotectants failed? Lessons learned from stroke trails. J Neurol 2005;252:1011–1020. [PubMed: 16133726]

27. Muller M, Somjen GG. Na+ and K+ concentrations, extra- and intracellular voltages and the effect of TTX in hypoxic rat hippocampal slices. J Neurophysiol 2000;83:735–45. [PubMed: 10669489]

28. Nishimura I, Ui-Tei K, Saigo K, Ishii H, Sakuma Y, Kato M. 17beta-estradiol at physiological concentrations augments Ca2+-activated K+ currents via estrogen receptor beta in the gonadotropin-releasing hormone neuronal cell line GT1-7. Endocrinol 2008;149:774–82.

29. Onitsuka M, Mihara S, Inokuchi H, Shigemori M, Higashi H. Mild hypothermia protects rat hippocampal CA1 neurons from irreversible membrane dysfunction induced by experimental ischemia. Neurosci Res 1998;30:1–6. [PubMed: 9572574]

30. Osuka K, Feustel PJ, Mongin AA, Tranmer BI, Kimelberg HK. Tamoxifen inhibits nitrotyrosine formation after reversible middle cerebral artery occlusion in the rat. J Neurochem 2001;76:1842–50. [PubMed: 11259502]

31. Plant K, Pelkey KA, Bortolotto ZA. Transient incorporation of native GluR2-lacking AMPA receptors during hippocampal long-term potentiation. Nat Neurosci 2006;9:602–4. [PubMed: 16582904]

32. Quintana P, Alberi S, Hakkoum D, Muller D. Glutamate receptor changes associated with transient anoxia/hypoglycaemia in hippocampal slice cultures. Eur J Neurosci 2006;23:975–983. [PubMed: 16519662]

33. Raffaelli G, Saviane C, Mohajerani MH, Pedarzani P, Cherubini E. BK potassium channels control transmitter release at CA3-CA3 synapses in the rat hippocampus. J Physiol 2004;557(Pt1):147–57. [PubMed: 15034127]

34. Raley-Susman KM, Kass IS, Cottrell JE, Newman RB, Chambers G, Wang J. Sodium Influx Blockade and Hypoxic Damage to CA1 Pyramidal Neurons in Rat Hippocampal Slices. J Neurophysiol 2001;86:2715–2726. [PubMed: 11731531]

35. Rasband, WS. ImageJ 1997–2004. National Institutes of Health; Bethesda, Maryland, USA: http;//rsb.info.nih.gov/ij/

36. Rossi DJ, Oshima T, Attwell D. Glutamate release in severe brain ischaemia is mainly by reversed uptake. Nature 2000;403:316–32. [PubMed: 10659851]
37. Rothman SM, Olney JW. Glutamate and the pathophysiology of hypoxic--ischemic brain damage. Ann Neurol 1986;19:105–11. [PubMed: 2421636]
38. Runden-Pran E, Hauq FM, Storm JF, Ottersen OP. BK channel activity determines the extent of cell degeneration after oxygen and glucose deprivation: a study in organotypical hippocampal slice cultures. Neuroscience 2002;112:277–88. [PubMed: 12044446]
39. Somogyi P, Klausberger T. Defined types of cortical interneurone structure space and spike timing in the hippocampus. J Physiol 2005;562:9–26. [PubMed: 15539390]Review
40. Sun X, Gu XQ, Haddad GG. Calcium influx via L- and N-type calcium channels activates a transient large-conductance Ca2+-activated K^+ current in mouse neocortical pyramidal neurons. J Neurosci 2003;23:3639–48. [PubMed: 12736335]
41. Sweeney MI, Yager JY, Walz W, Juurlink BH. Cellular mechanisms involved in brain ischemia. Can J Physiol Pharmacol 1995;73:1525–35. [PubMed: 8789404]
42. Taylor CP, Weber ML. Effect of temperature on synaptic function after reduced oxygen and glucose in hippocampal slices. Neuroscience 1993;52:555–62. [PubMed: 8450958]
43. Thompson RJ, Zhou N, MacVicar BA. Ischemia Opens Neuronal Gap Junction Hemichannels. Science 2006;312:924–927. [PubMed: 16690868]
44. Van Hooijdonk CA, Glade CP, Van Erp PE. TO-PRO-3 iodide: a novel HeNe laser-excitable DNA stain as an alternative for propidium iodide in multiparameter flow cytometry. Cytometry 1994;17:185–189. [PubMed: 7530620]
45. Wade GN, Blaustein JD, Gray JM, Mertrdith JM. ICI 182, 780: a pure antiestrogen that affects behaviors and energy balance in rats without acting in the brain. Am J Physiol 1993;265:1392–1398.
46. Wakade C, Khan MM, De Sevilla LM, Zhang QG, Mahesh VB, Brann DW. Tamoxifen neuroprotection in cerebral ischemia involves attenuation of kinase activation and superoxide production and potentiation of mitochondrial superoxide dismutase. Endocriol. 2008Epub 2007 Sep 27
47. Xie MJ, Wang W, Kimelberg HK, Zhou M. Oxygen and glucose deprivation induced changes in astrocyte membrane potential and their underlying mechanisms in acute rat hippocampal slices. J Cereb Blood Flow Metab 2008;28:456–67. [PubMed: 17713462]
48. Zhang H, Schools GP, Tin L, Wei W, Kimelberg HK, Zhou M. Resveratrol attenuates early pyramidal neuron excitability impairment and death in acute rat hippocampal slices caused by oxygen-glucose deprivation. Exp Neurol 2008;212:44–52. [PubMed: 18495119]
49. Zhang Y, Jin Y, Behr MJ, Feustel PJ, Morrison JP, Kimelberg HK. Behavioral and histological neuroprotection by tamoxifen after reversible focal cerebral ischemia. Exp Neurol 2005;196:41–6. [PubMed: 16054626]
50. Zhou M, Schools GP, Kimelberg HK. Development of GLAST (+) astrocytes an NG2 (+) glia in rat hippocampus CA1: mature astrocytes are electrophysiologically passive. J Neurophysiol 2006;95:134–43. [PubMed: 16093329]

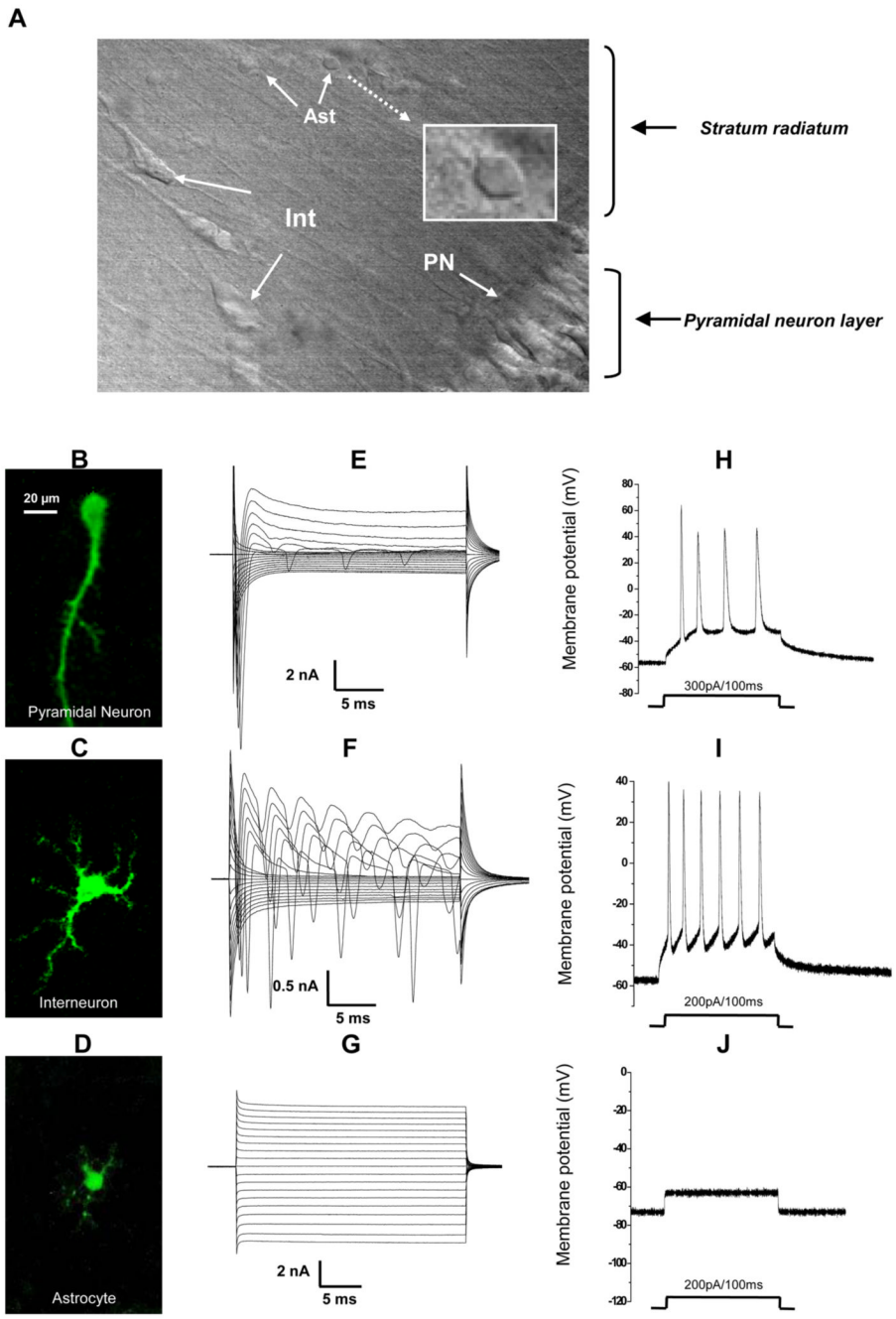

Figure 1. Identification of pyramidal neurons, interneurons and astrocytes in the stratum radiatum of rat hippocampus CA1 region

A. DIC image of a portion of the CA1 region in an acute hippocampal slice showing the pyramidal neuron layer, interneurons (Int) and astrocytes (Ast) located in the *stratum radiatum*. The morphology of an astrocyte soma is shown in expanded scale in the white framed inset in **A. B** – **D**. Biocytin-Cy2 images of a representative pyramidal neuron (**B**), interneuron (**C**) and astrocyte (**D**). Biocyin (0.1%) was loaded into the cells during whole-cell recordings. The scale bar in **B** also applies to **C** and **D**. Whole-cell voltage clamp recordings in **E–G** and current clamp recordings in **H–J** were all obtained from the same pyramidal neuron, interneuron and astrocyte shown in **B**–**D**, respectively. For whole-cell voltage-clamp recording,

the cells were held at −70 mV at resting and stepped from −160 mV to +20 mV (10 mV increments, 25 ms duration, with a 1-second interval between the consecutive voltage steps). The pyramidal neuron (**E**) and interneuron (**F**) are characterized by large depolarization step-activated inward Na^+ and voltage-gated K^+ channel currents. The interneuron also shows regenerative inward Na^+ channel currents within the same 25 ms time scale. **G**. Astrocytes are characterized by a linear I–V relationship, predominantly K^+ currents. In current clamp recording, positive current injection (as indicated below **H**–**J**) induces action potential spikes from both pyramidal neurons (**H**) and interneurons (**I**). Astrocytes show no regenerative spikes with the same positive current injection (**J**).

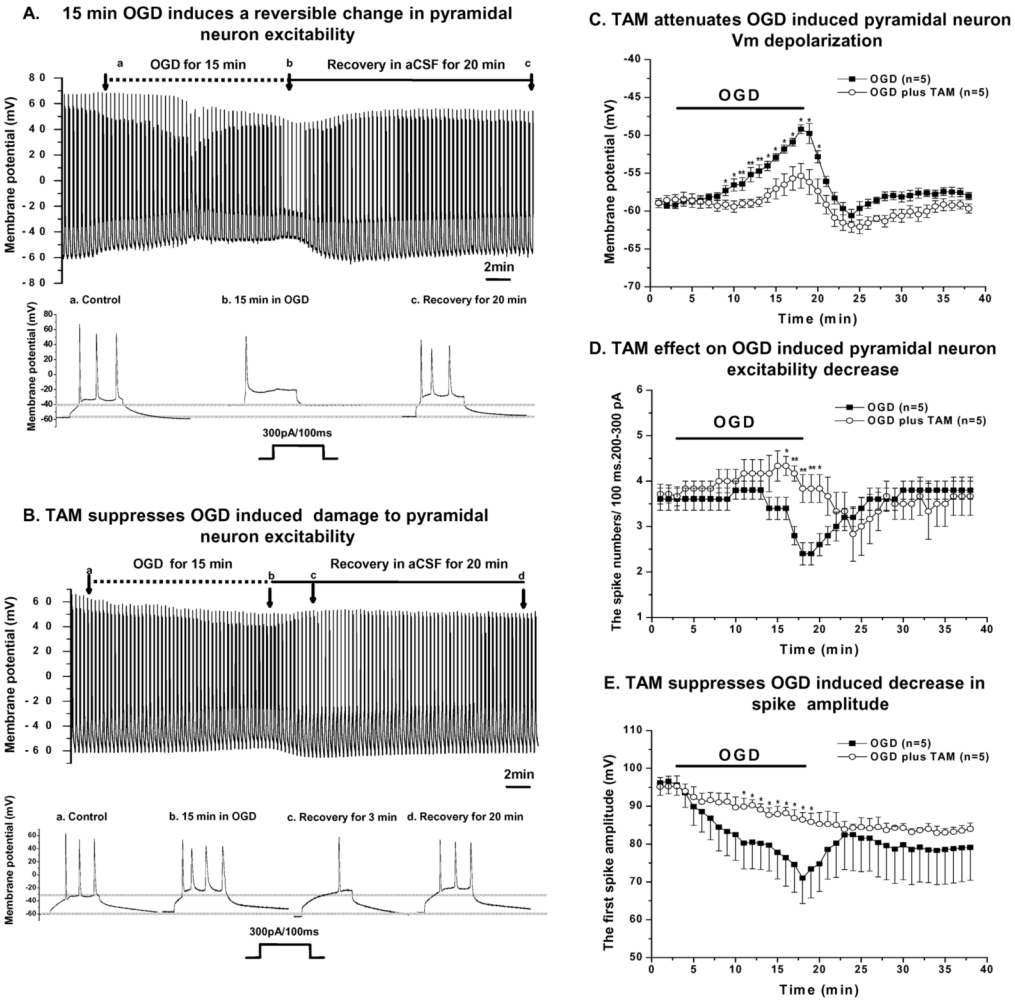

Figure 2. Attenuation of OGD- induced impairment of pyramidal neuron excitability by TAM

A. OGD-induced changes in pyramidal neuron electrophysiology recorded in current clamp mode. During the pre-OGD control period, OGD period and recovery from OGD period, the Vm and excitability changes were periodically measured every 20 seconds by delivering a 200–300pA/100 ms duration current pulse to the recorded cell. Representative traces from the control, OGD and recovery phases, as indicated by the arrows, are displayed in the expanded scale in the lower panel in **A**, showing the marked Vm depolarization and loss of spike number over a 15 min. OGD insult. **B**. In the presence of 10 μM TAM the Vm was maintained, as shown in another pyramidal neuron recording (**a–c** in the lower panel in **B**). TAM also caused a Vm hyperpolarization after the recorded cell was returned to the normal aCSF with a concomitant decrease in spike number (d in **B**). Comparisons of OGD-induced impairment and TAM's effect on pyramidal neuron Vm (**C**), spike number (**D**) and first spike amplitude (**E**) over the course of 15 min.OGD. 0.1% DMSO, used as solvent for TAM, was applied with 15 min OGD in the control group. (**D**) The number of action potential spikes was significantly reduced in the OGD group and was completely reversed after OGD withdrawal. With TAM present, the spike number was actually increased slightly during OGD and decreased significantly in the initial post-OGD period, corresponding to the Vm hyperpolarization in the same recovery phase. The spike number returned fully to the control level at the end of the 20 min. recovery period. (**E**) OGD caused a time-dependent decrease in action potential spike amplitude that was largely prevented by TAM. The gradual further decrease in spike amplitude

in the recovery time period after OGD was likely also attributable to the TAM-induced membrane potential hyperpolarization. * and ** indicate that at the given time point the differences between two groups are statistically significant at the level of $p<0.05$ and $p<0.01$, respectively.

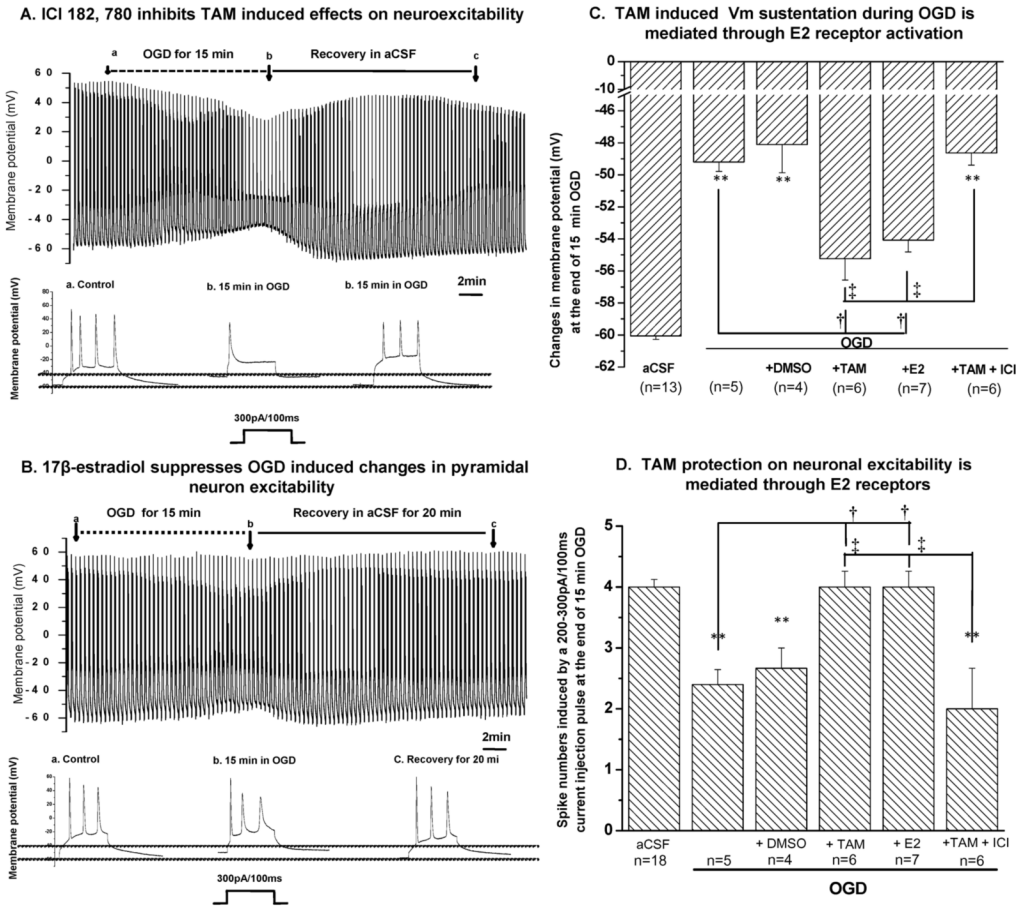

Figure 3. Acute TAM action is mediated through estrogen receptor activation

A. Pyramidal neuron OGD responses with the same recording protocol as described in Fig. 2, in the presence of 10 μM TAM and the estrogen receptor inhibitor ICI 182,780 (1μM), which completely inhibited TAM mediated effect (shown in expanded trace in b below **A** to compare with Fig. 3**B**). **B.** β-estradiol (1 μM) produced a similar effect as compared with TAM (Fig. 3B). **C** and **D** summarizes all the data on neuronal Vm (**C**) and spike numbers (**D**) under the different conditions indicated. ** indicates that the differences between control in aCSF and other conditions were statistically significant at $p<0.01$. Tukey's HSD test was performed for multiple comparisons amongst OGD, OGD+DMSO, OGD+TAM, OGD+E2 and OGD+TAM +ICI groups for data presented in **C** and **D**. The significant differences between OGD and OGD +TAM groups, and between OGD and OGD+E2 groups are indicated as †, and the significant differences between OGD+TAM and OGD+TAM+ICI groups, and between OGD+E2 and OGD+TAM+ICI groups are indicated as ‡.

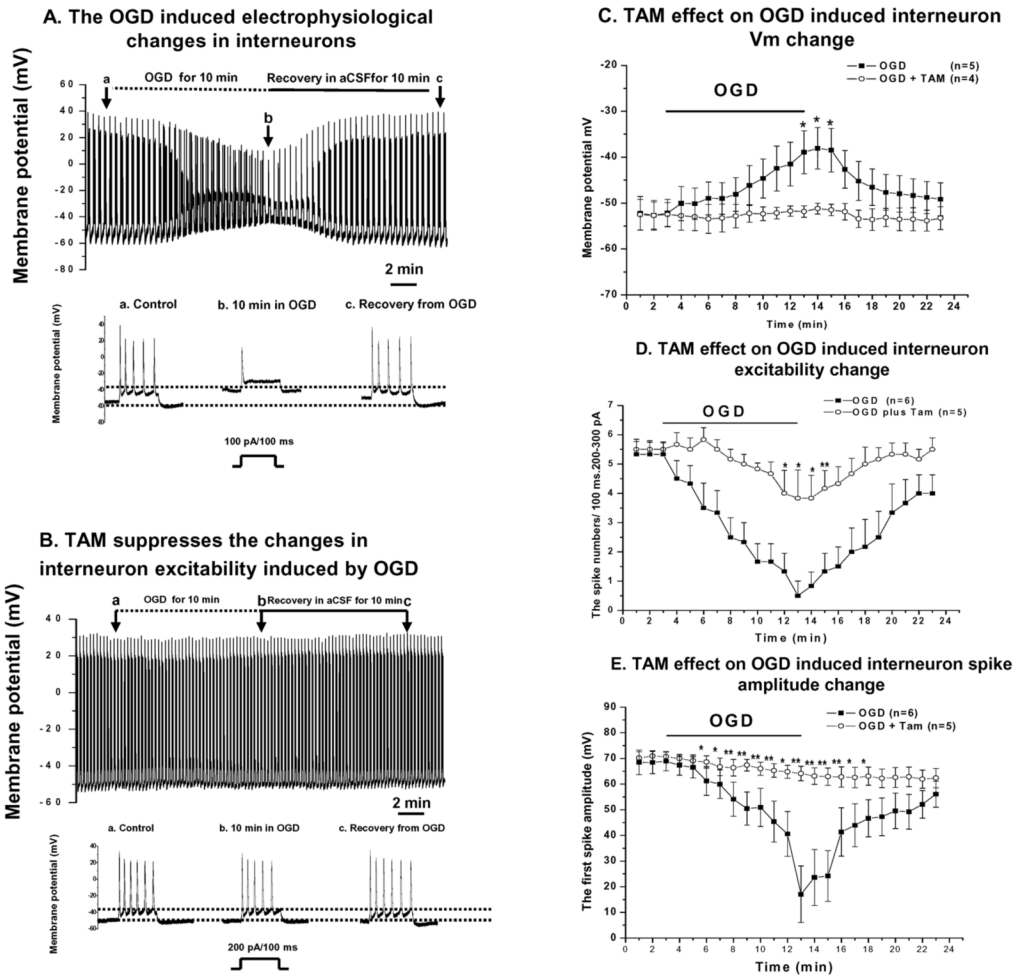

Figure 4. TAM effects on interneurons

The recording procedure is the same as in Figs. 2 and 3, except the OGD exposure was reduced to 10 min. and the amount of positive current injected was less (100 pA–200 pA *vs.* 200 pA – 300 pA). **A**. Shows typical OGD-induced changes in interneuron electrophysiology. Representative time-expanded traces in the lower panel in **A** are selected from the control, OGD and post-OGD recovery period in aCSF as indicated by the arrows marked **a**, **b** and **c** in the top recording. Interneurons appear to be more susceptible than pyramidal cells to OGD, since during a 10 min. OGD the Vm depolarized continuously and the decline in spike number and amplitudes with time was greater. However, all of these OGD induced changes were reversible upon OGD withdrawal (**a–c** in the lower panel in **A**). In the presence of TAM (10 μM), the interneuron did not show any Vm depolarization during OGD. The decline in spike numbers was also largely absent and the amplitude of the first spike was essentially not changed (**B** and representative traces below **B**). **C–E** summarizes the TAM effects on the three parameters as described for Fig. 2. TAM maintained the Vm repolarization (**A**) and also showed strong effects on interneuron spike number (**B**) and amplitude (**C**). * and ** indicate the differences between OGD and OGD+TAM groups at the indicated time points were significant at the levels of $p<0.05$ and $p<0.01$, respectively.

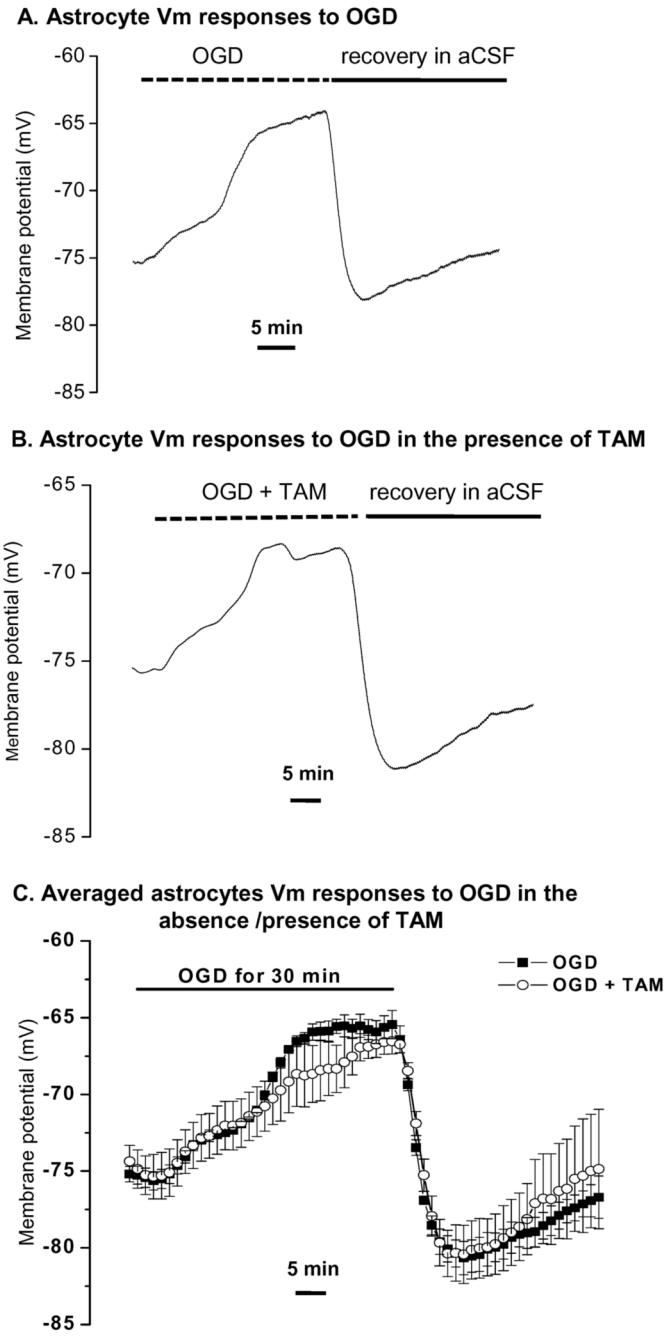

Figure 5. OGD- induced astrocyte Vm depolarization was not affected by TAM

A. Shows a typical astrocyte Vm response to 30 min. OGD treatment in current clamp recording that is characterized by a progressively depolarizing Vm, reflecting stages of increasing extracellular [K^+] as previously shown by Xie et al., (2008). **B**. Shows another astrocyte Vm response to OGD in the presence of 10 μM TAM. **C.** Summary plots showing changes in OGD induced astrocyte Vm were unaffected by TAM (n=3 for each plot).

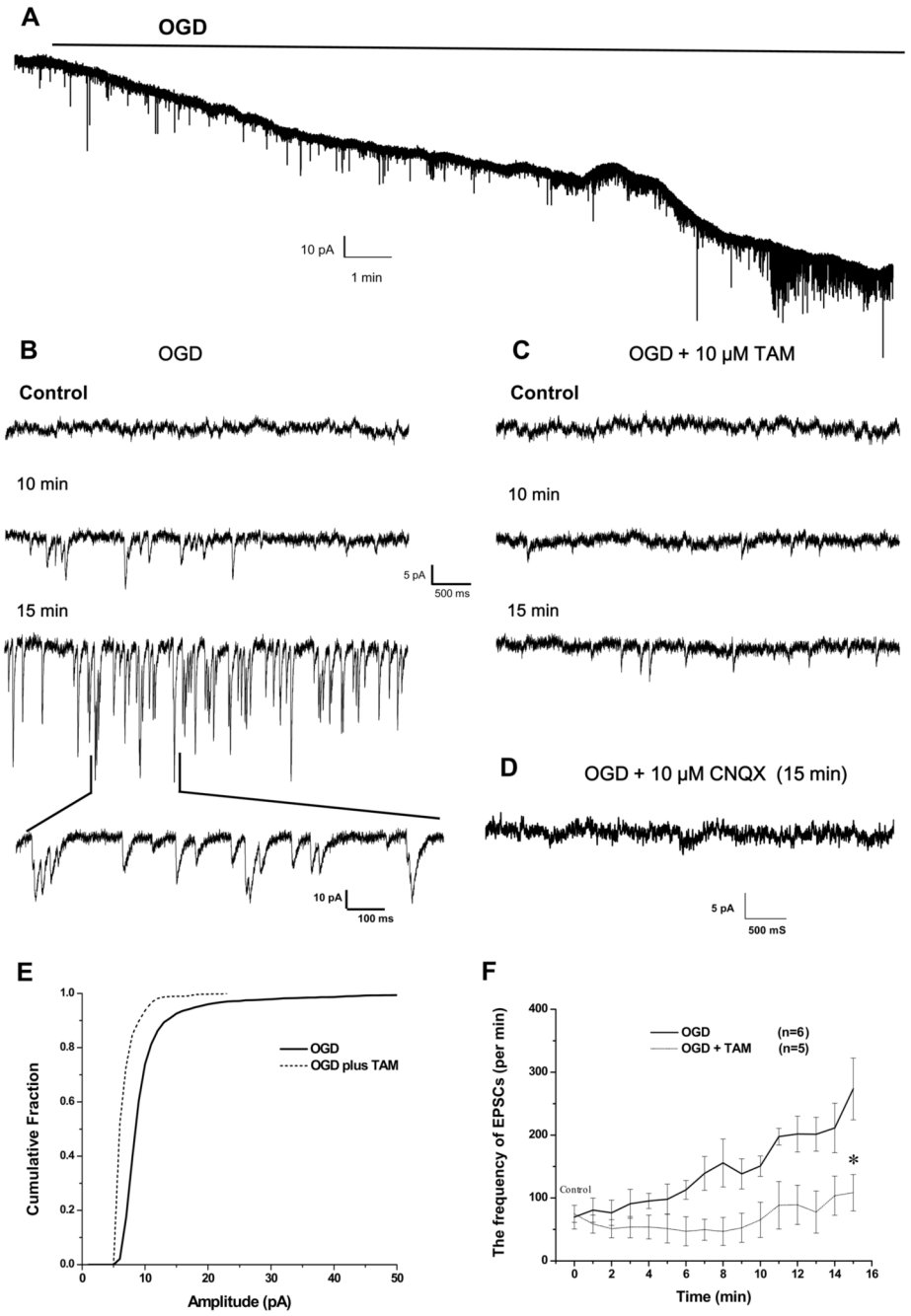

Figure 6. Tamoxifen attenuates the OGD-induced increased EPSCs in pyramidal neurons

A. Pyramidal neuron responses to a15 min.OGD treatment in voltage clamp recording at the holding potential of −60 mV, showing the time-dependent downward shift in holding currents (reflecting the Vm depolarization as shown in Fig 2A in the current clamp recording). This is accompanied by an increase in the frequency and amplitude of the spontaneous EPSCs (sEPSCs, downward current deflections). **B**. Shows OGD induced excessive sEPSCs at different OGD treatment time points, in an expanded scale. **C**. In the presence of 10 μM TAM, the OGD-induced sEPSCs were almost completely inhibited. **D**. Shows inhibition of sEPSCs by the AMPA receptor blocker CNQX. **E**. Comparison of cumulative probability of sEPSC amplitudes between the control OGD (solid line) and OGD plus TAM (dashed line). The data

used were taken from **B** and **C** at 15 min. OGD treatment. **F**. Summary of all the experiments showing that the OGD-induced increase in sEPSC frequency is completely inhibited by 10 μM TAM. For the analyses presented in **D** and **E**, only downward current deflections greater than −5 pA from the baseline in all the recordings were considered as acceptable sEPSC events and were included for these analyses.* indicates that the differences in between OGD and OGD + TAM groups was statistically significant at the $p < 0.05$.

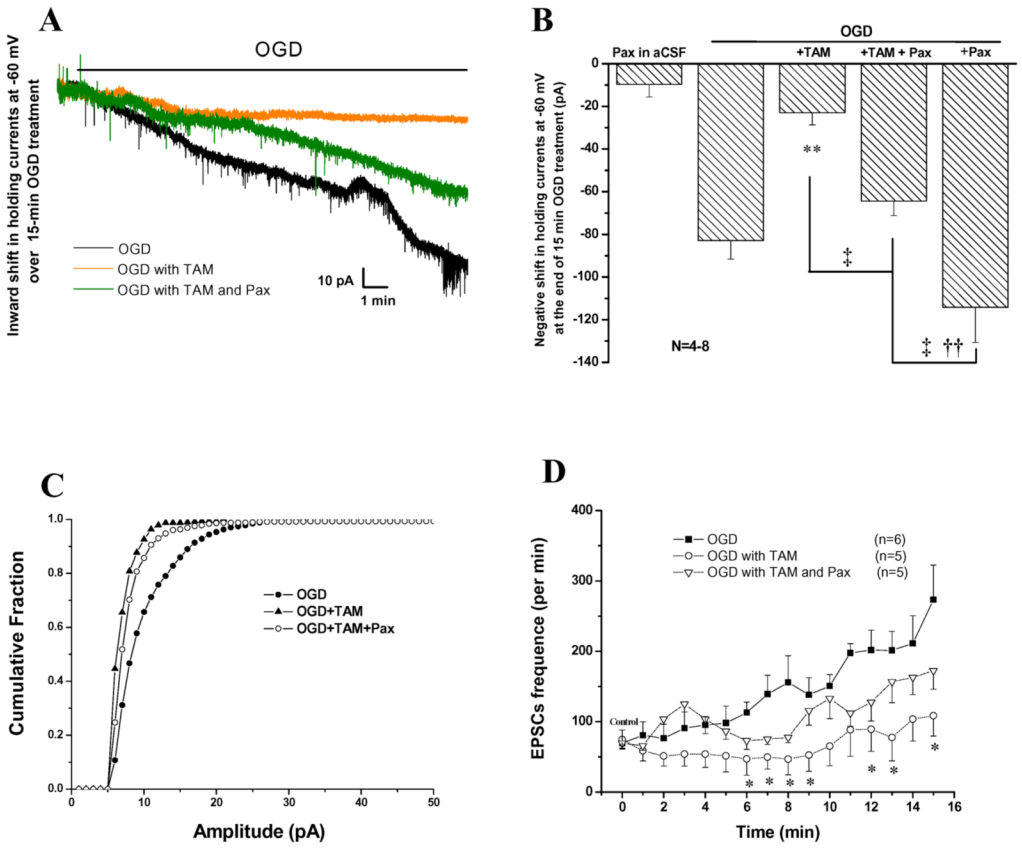

Figure 7. TAM mediated neuronal Vm maintenance is partially mediated by activation of BK channels

A. Voltage-clamp recordings of CA1 pyramidal neurons exposed to a 15 min.OGD treatment at −60 mV holding potential. As indicated in **A**, the black, green and orange traces are representative recordings under conditions of OGD, OGD+TAM (10μM) + Pax (10μM) and OGD +TAM (10μM), respectively. The relative speed and degree of Vm depolarization under these recording conditions were proportional to the slope and amplitude of the holding inward currents. The OGD induced large inward current (black) was substantially inhibited by TAM (orange), which was partially inhibited by Pax (green). **B**. Summary of all the experiments including additional controls of Pax alone in control aCSF and Pax + OGD. Pax alone did not result in a significant negative shift in holding currents (−9.6 ± 5.9 pA). OGD alone induced a −82±8.7 pA negative shift in holding currents that was markedly reduced by TAM (−23 ± 5.7 pA). The TAM effect was partially blocked by Pax (−64.4 ± 6.8 pA). Pax itself markedly negatively shifted OGD induced inward holding currents (−114 ± 16.5 pA). Tukey's HSD test was performed for multiple comparisons amongst OGD, OGD+TAM, OGD+TAM+Pax and OGD+Pax groups. The significant ($p < 0.05$) differences between OGD, OGD+TAM and OGD +TAM+Pax with other groups are indicated by **, † and, ‡, respectively. In the presence of Pax, TAM inhibition of OGD induced sEPSCs was largely reversed. **C** The cumulative fraction of sEPSCs in **C** was calculated and compared as for Fig. 6. **D**. the OGD induced sEPSCs increase was only partially inhibited in OGD+TAM+Pax group, 172 ± 26.5/min, as compared to OGD +TAM at 108 ± 28.8/min, all at the end of 15 min. OGD treatment. * in **D** indicates the difference between OGD and OGD+TAM, or OGD and OGD+TAM+Pax at a given time point during a 15 min. OGD treatment is statistically significant at $p < 0.05$, determined by one-way ANOVA test.

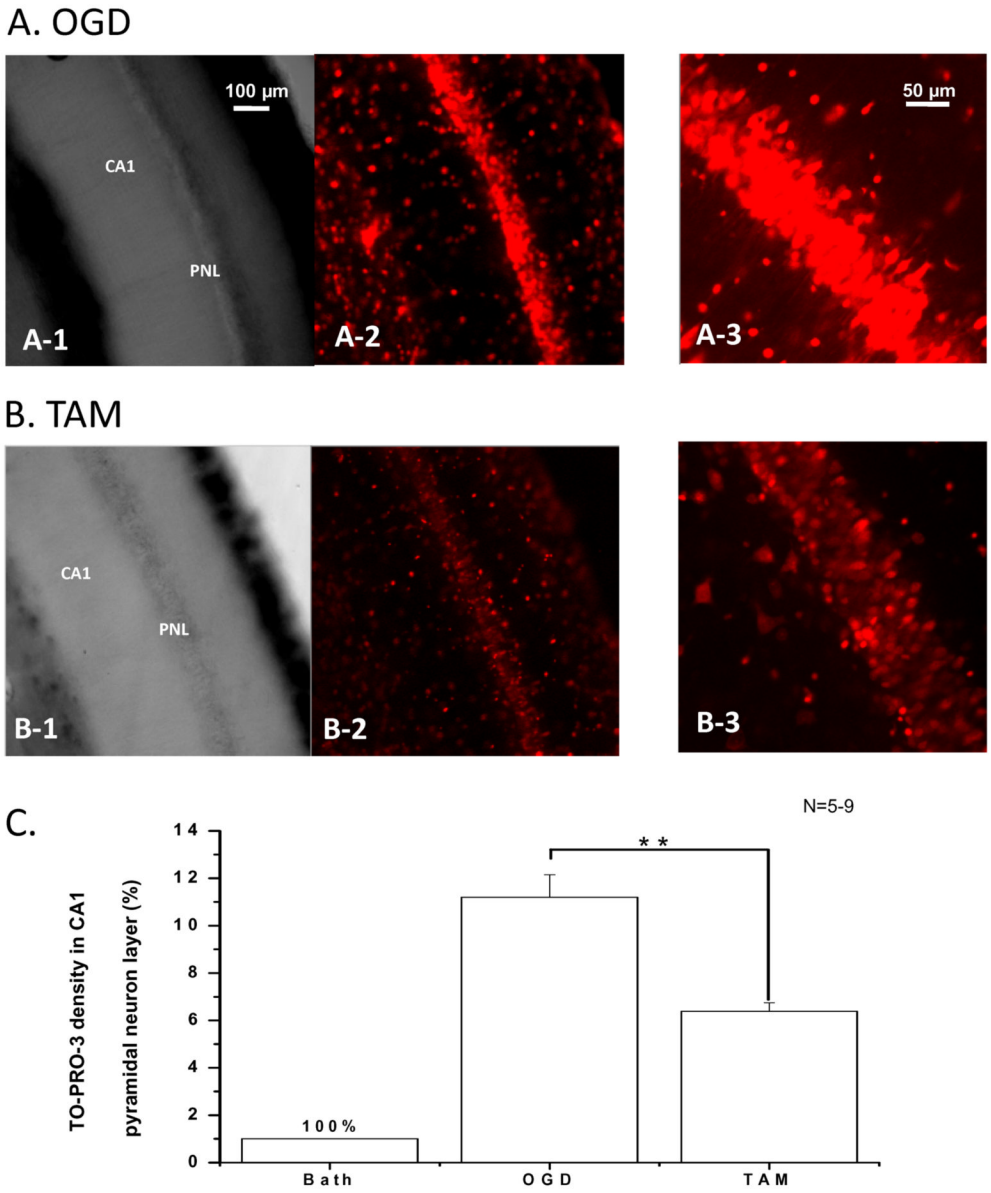

Figure 8. OGD induced neuronal death in hippocampal CA1 region was largely reduced by TAM treatment

A. OGD induced neuronal damage in the CA1 region in an acutely prepared rat hippocampal slice. The bright field image of this region acquired with a 10X objective is shown in **A**-1 after 20 min exposure to OGD, and the TO-PRO-3-I staining fluorescence image of the same field is shown in **A**-2. TO-PRO-3-I staining in pyramidal neuron layer (PNL) using a 25X objective is shown in **A**-3. **B**. With addition of 10 μM TAM in OGD solution for the same 20 min OGD exposure, the number of TO-PRO-3-I stained cells in the pyramidal neuron layer were markedly reduced (**B**-2, 3). **C**. Quantitative analyses of the pyramidal neuronal death in the absence and presence of TAM with the same 20 min OGD treatments are shown in C. Compared to control TO-PRO-3-I staining, 20 min OGD induced an 11.2 ± 0.9 fold (n=6) increase in the staining density in the CA1 pyramidal neuron layer that was reduced to 6.4 ± 0.4 fold (n=9) by 10 μM TAM. Bars represent the mean±SEM, ** indicates that the differences between OGD and OGD +TAM was statistically significant at the level of $p<0.01$.